(Preprint) AAS 19-TBD

PERFORMANCE IMPROVEMENTS FOR THE LUNAR RECONNAISSANCE ORBITER GYROLESS EXTENDED KALMAN FILTER

Julie Halverson (formerly Thienel),* Oscar Hsu,† Philip Calhoun,‡ and Yohannes Tedla,§

In late 2017, the laser intensity monitor (LIM) current began to decline on the Lunar Reconnaissance Orbiter (LRO) miniature inertial measurement unit (MIMU). The MIMU was powered off in March 2018 and has only been used during extended eclipses, a pre-eclipse orbit phasing maneuver, and critical momentum unloads. Science slews were suspended, and the onboard extended Kalman filter (EKF) was disabled. A coarse rate was estimated through star tracker quaternion differentiation, and attitude was provided directly from a single star tracker. A complementary filter, combining the differentiated quaternions with the integrated acceleration derived from the attitude control torque, was developed, tested, and uploaded to the spacecraft in December, 2018. The EKF has been enabled, using the complementary filter rate in place of the MIMU and science slews are now being performed. This paper presents an overview of the complementary filter rate estimation and EKF changes, fault detection updates without the MIMU, and inflight performance improvements.

INTRODUCTION

The Lunar Reconnaissance Orbiter (LRO) was launched on June 18, 2009 and is currently in its fourth extended science mission phase. LRO is equipped with seven instruments: Cosmic Ray Telescope for the Effects of Radiation (CRaTER), Diviner Lunar Radiometer (DLRE), Lyman Alpha Mapping Project (LAMP), Lunar Exploration Neutron Detecter (LEND), Lunar Orbiter Laser Altimeter (LOLA), Lunar Reconnaissance Orbiter Camera (LROC), and the mini-RF technology demonstration. The LRO orbit is an approximately 30 km by 200 km altitude elliptical orbit with an inclination of approximately 86 deg and orbital period of 2 hours. The primary orientation is nadir pointing, with frequent slews off nadir to support various science observations and instrument calibrations.

Figure 1 is an image of the LRO spacecraft. LRO has two star trackers, and a single miniature inertial measurement unit (MIMU). An extended Kalman filter estimates the spacecraft attitude using the star tracker quaternions and the MIMU data. The attitude control system has four modes of operation: Observing, Momentum Management, Orbit Maintenance, and Sun Safe. The Attitude Control System (ACS) is 3-axis stabilized, and the primary Observing mode provides nadir, off-nadir, and inertial fine pointing in support of science observations, instrument calibrations, and

*Space Sciences Mission Operations, NASA/GSFC, Greenbelt, MD 20771.
†Guidance, Navigation, and Control, NASA/GSFC, Greenbelt, MD 20771.
‡Guidance, Navigation, and Control, NASA/GSFC, Greenbelt, MD 20771.
§KBRWyle, Greenbelt, MD 20771.

special imaging. LRO has a set of four reaction wheels and a reaction control system for momentum unloading.[1]

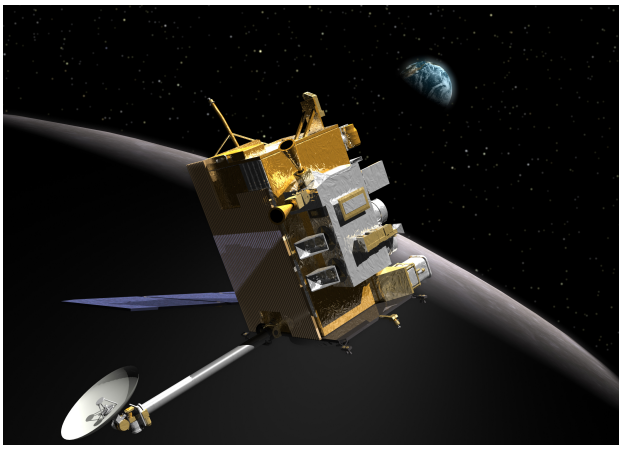

Figure 1: Lunar Reconnaissance Orbiter (Courtesy of NASA/LRO)

In late 2017, the MIMU laser intensity monitor (LIM) current on the X axis began declining. In March 2018, the MIMU was powered off. The EKF was disabled and all slews were suspended, the spacecraft maintained nadir pointing. The MIMU was powered on during the long eclipses in July 2018 and January 2019 and was used during a pre-eclipse orbit phasing maneuver. If a fault occurs on the spacecraft, the MIMU will be powered on and the spacecraft will slew to a sun pointing orientation. In 2014, a preliminary study indicated that applying a complementary filter to the star tracker differentiated quaternions and the commanded wheel torque could result in a rate estimate to replace the MIMU in the EKF.[2] The complementary filter was incorporated into the High Fidelity (HiFi) simulator used for guidance, navigation, and control (GNC) testing during the LRO development and the EKF was configured to accept the estimated rate in place of the MIMU. Comprehensive Monte Carlo testing was completed, which included numerous slew scenarios based on actual science slews. The complementary filter and EKF updates were then incorporated into flight software (FSW), ground tested, and successfully uploaded to the spacecraft in December 2018.[3] The gyroless EKF was enabled and a series of test slews were conducted.

The remaining sections of this paper include an overview of the complementary filter and EKF, inflight commissioning activities, fault detection improvements, and performance improvements.

OVERVIEW OF COMPLEMENTARY FILTER AND EXTENDED KALMAN FILTER

Complementary Filter

The quaternion kinematics, given in equation 1, and Euler's equation, given in equation 2, are both a function of the angular velocity.

$$\dot{q} = \frac{1}{2} Q(q)\omega \tag{1}$$

$$T = \frac{d}{dt}(I\omega + h) + \omega \times (I\omega + h) \tag{2}$$

where q is the quaternion, $Q(q)$ is a 4×3 matrix, ω is the angular velocity, T is torque, I is the spacecraft inertia, and h is the reaction wheel angular momentum.

The Observing mode attitude controller is a quaternion-feedback, proportional-integral-derivative (PID) controller designed to produce reaction wheel torque commands. The estimated gyroscopic torque is added to the PID control torque which is then filtered, transformed into the reaction wheel frame, and adjusted for reaction wheel drag. The final wheel torque commands are limited and then redistributed to the wheels with the Mini-Max wheel momentum redistribution.[4]

Without the MIMU, an alternative method for rate estimation is necessary. A complementary filter is a method of combining two different measurement sources to estimate a single variable, when the two measurements have different frequency characteristics.[5] The first measurement is derived from equation 1

$$\hat{\omega} = 2Q(q_{ST})^T \dot{q}_{\mathrm{ST}} \tag{3}$$

where q_{ST} indicates the quaternion from a star tracker (ST). The second measurement, given in Equation 4, is obtained by integrating the angular acceleration calculated from the spacecraft inertia (inverse) and the PID controller estimated wheel torque.

$$\hat{\dot{\omega}} = I^{-1}(-T_{\mathrm{m}} - T_{\mathrm{ffwd}}) \tag{4}$$

where T_{m} is the commanded wheel torque, with the drag compensation removed, transformed into the body frame. T_{ffwd} is the gyroscopic torque from equation 2 which is also removed. The complementary filter applied to LRO minimizes the low frequency noise from the quaternion differentiation and the high frequency noise from the controller estimated torque. Equation 5 is a conceptual expression of the complementary filter in the frequency domain.

$$\hat{\omega}(s) \approx \frac{\omega}{s+\omega}\left[(2Q^T sq(s)\right] + \frac{s}{s+\omega}\left[\frac{1}{s}(I^{-1}T)\right] \tag{5}$$

The complementary filter is implemented inflight using an existing second order discrete filter. The details of the complementary filter design are presented in [3].

EKF Overview and Algorithm Updates

The EKF filter traces its history to an algorithm proposed by Murrell in 1978.[6] Murrell proposed a Kalman filter design for the attitude determination that utilized scalar updates, avoiding matrix inversion and reducing the computational load. Several NASA missions made use of this onboard filter, including the Tropical Rainforest Measuring Mission (TRMM), Wilkinson Microwave Anisotropy Probe (WMAP) and the Solar Dynamics Observatory (SDO). The LRO EKF is based heavily on the TRMM and WMAP filters.

The EKF is implemented as a discrete Kalman filter following the standard equations for covariance propagation and state and covariance update.[7]

$$P_k(-) = \Phi_{k-1} P_{k-1} \Phi_{k-1}^T + Q_{k-1} \tag{6}$$

$$K_k(-) = P_k H_k^T [H_k P_k H_k^T + R]^{-1} \tag{7}$$

$$\underline{\hat{x}}_k(+) = \underline{\hat{x}}_k(-) + K_k[\underline{z}_k - H_k \underline{\hat{x}}_k(-)] \tag{8}$$

$$P_k(+) = [I - K_k H_k] P_k(-) \tag{9}$$

Where P is the covariance matrix of the error states, Q is the process noise covariance matrix, Φ is the state transition matrix, K is the Kalman gain, H is the measurement matrix, R is the

measurement noise covariance matrix, $\underline{z}$ is the effective measurement, and $\underline{x}$ is the error state vector. The $\hat{}$ refers to an estimated quantity, $(+)$ refers to a posteriori estimates and $(-)$ refers to a priori estimates.

The gyro based EKF filter states consists of the attitude quaternion and gyro bias. The attitude quaternion is propagated according to equation 3 and the bias is modeled as a random walk.

$$\dot{\underline{b}} = \underline{\eta}_u \tag{10}$$

The gyro model is given as

$$\underline{\omega}_g = \underline{\omega} + \underline{b} + \underline{\eta}_v \tag{11}$$

The terms $\underline{\eta}_u$ and $\underline{\eta}_v$ are Gaussian distributed white noise vectors with zero mean and standard deviations given by $\underline{\sigma}_u$ and $\underline{\sigma}_v$, respectively. In the gyroless EKF, the gyro data, $\underline{\omega}_g$ is replaced with the rate estimate from the complementary filter

$$\hat{\underline{\omega}}_g = \sum_{i=1}^{n} \hat{\underline{\omega}}_{ST,i} + \hat{\underline{\omega}}_{RW} \tag{12}$$

where n is either 1 or 2, depending on the number of star tracker quaternions available. The rest of the EKF algorithm is unchanged. The state is updated with the measurements from the star trackers. The star tracker quaternions are transformed into the body frame and then used to generate a measurement of the attitude error.

INFLIGHT COMMISSIONING ACTIVITIES

The FSW patch containing the complementary filter and revised EKF was loaded, installed, and activated on LRO in December 2018. The installation was done with LRO in the sun safe mode. The MIMU was on during the installation and slew back to nadir pointing. The complementary filter rate was selected as the rate source, the EKF was enabled, and the MIMU was powered off. Figure 2 shows the immediate improvement in the attitude control error during the first test operation of the EKF.

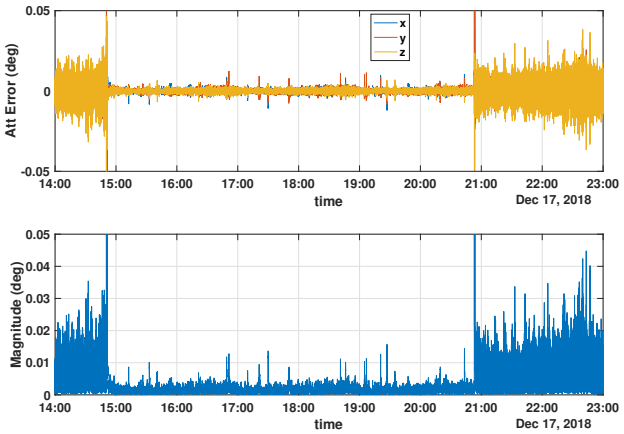

Figure 2: Onboard Attitude Error With EKF Enabled (approximately 15:00 to 21:00)

.

Several months were dedicated to evaluating the EKF performance and selectively performing test slews. First small test slews of five degrees were successfully performed in each spacecraft

direction, followed by a 30 deg test roll slew. There was interest in using the LROC to image the landing site of the Chang'e 4 lander,[8] so the first large science slew was a 60 deg roll slew in late January. Figure 3 shows the attitude and rate controller errors (magnitudes) during the slew. Figure 4 is the resulting LROC image, the first LRO science slew since March 2018. The landing site is just visible in this wide field image. Several subsequent images have been captured and are featured at [9].

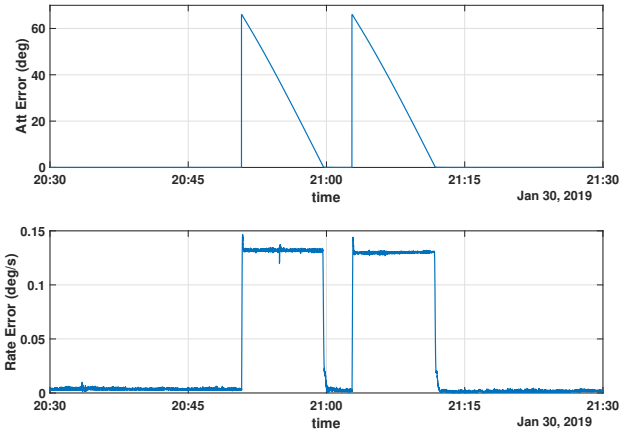

Figure 3: Attitude and Rate Error Magnitudes During First Large Slew

.

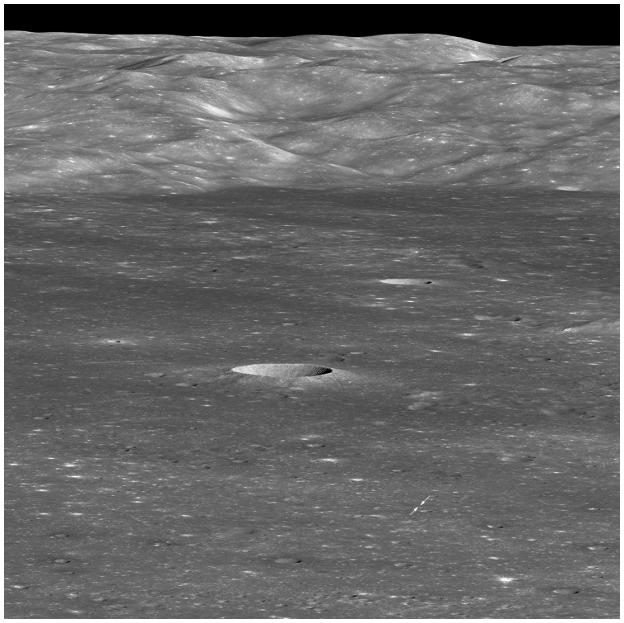

Figure 4: First Large Slew, LROC Image, Landing Site Identified by Small Arrows. (Courtesy of NASA/GSFC/Arizona State University)

In addition to slew testing, the EKF and controller performance has been analyzed. Spikes were visible in the attitude control errors and may be due to inaccuracies in the onboard wheel drag model, particularly the Coulomb friction term. Figure 5 is an example of the increase in attitude error fol-

lowing a zero wheel speed crossing. The final paper will provide the results showing improvement in performance after updating the onboard reaction wheel drag model.

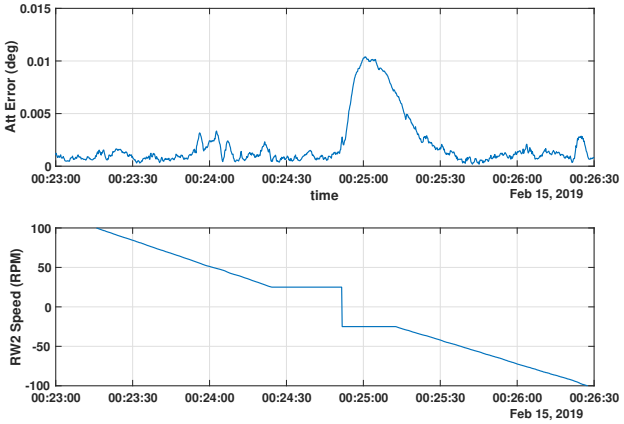

Figure 5: Attitude Error and Reaction Wheel 2 Speed Crossing Zero

.

Additional improvements are planned in the EKF tuning. In particular, the angle random walk and rate random walk terms, σ_v and σ_u in equations 10 and 11, respectively, will be updated to improve performance. Similarly, the star tracker measurement noise will also be updated based on EKF performance.

UPDATES TO FAULT DETECTION

The first update to fault detection was to smoothly transition to a valid star tracker attitude should a fault occur in the EKF. When the MIMU provided the rate source, the attitude could be propagated for an extended period on the MIMU if an EKF fault occurred. Without the MIMU, attitude and rate errors grow quickly when propagating on the noisier EKF estimated rate, so a switch is made to a star tracker attitude if the EKF fault cannot be quickly cleared.

It was discovered during ground testing that large attitude and rate errors occur if both star trackers are invalid for an extended period of time.[3] Indications of this have been observed inflight when a star tracker is occulted and the other star tracker experiences a brief drop in quaternion quality. Figure 6 shows the increase in attitude error when one star tracker was occulted and there was a single (0.2 sec) drop in validity of the other star tracker. In addition to regular occultations, the star trackers occasionally reset due to single event upsets. It can take 30 seconds or more to restore the star tracker following a reset. Should this occur while the other star tracker is occulted, large attitude and rate errors will accumulate likely tripping fault detection limits that would transition LRO to safe mode. Preliminary ground testing indicates that disabling the controller during the period of simultaneous invalid star tracker data greatly reduces the errors and avoids tripping attitude and rate error fault detection limits. The final paper will include the testing and uploading of onboard fault detection checks that will temporarily disable the PID control during simultaneous star tracker outages lasting more than a few seconds.

REFERENCES

[1] P. C. Calhoun and J. C. Garrick, "Observing Mode Attitude Controller for the Lunar Reconnaissance Orbiter," NASA Technical Reports Server, March 2008. https://ntrs.nasa.gov.

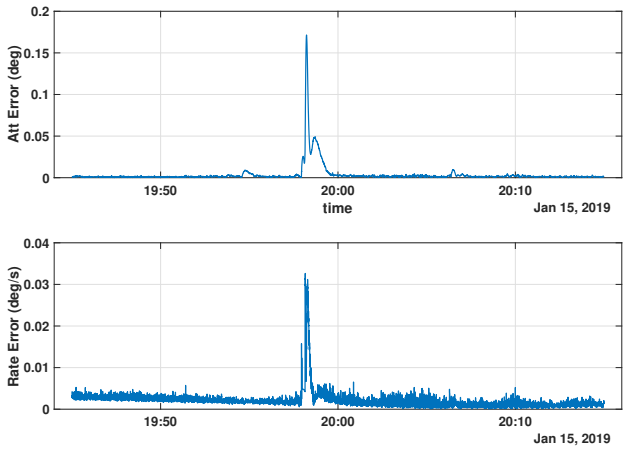

Figure 6: Attitude Error and Rate Error During Short Simultaneous Star Tracker Outage

.

[2] P. Calhoun, "MIMU Failure Risk Mitigation Trade Study, ST Derived Rates for Use in LRO Observing Mode," Presentation, August 2014. Internal NASA Goddard Space Flight Center document.

[3] J. Halverson, P. Calhoun, O. Hsu, J.-E. Dongmo, R. Besser, B. Ellis, R. DeHart, Y. Tedla, S. Rosney, and S. Snell, "Testing of the Lunar Reconnassiance Orbiter Attitude Control System Re-Design Without a Gyro," *AAS Guidance and Control Conference*, Breckenridge, Colorado, February 2019.

[4] F. L. Markley and J. L. Crassidis, *Fundamentals of Spacecraft Attitude Determination and Control*. Springer, 2014.

[5] S. Park and J. How, "16.333: Lecture 15, Inertial Sensors, Complementary filtering, Simple Kalman Filtering," Presentation, 2004. https://ocw.mit.edu/courses/aeronautics-and-astronautics/16-333-aircraft-stability-and-control-fall-2004/lecture-notes.

[6] J. W. Murrell, "Precision Attitude Determination for Multimission Spacecraft," *AIAA Guidance and Control Conference*, Palo Alto, California, August 1978.

[7] J. Halverson, R. Harman, R. Carpenter, and D. Poland, "Tuning the Solar Dynamics Observatory Onboard Kalman Filter," *AIAA/AAS Astrodynamics Specialist Conference*, No. AAS 17-591, Stevenson, Washington, August 2017.

[8] "Astronomy Picture of the Day," website. https://apod.nasa.gov/apod/ap190105.html.

[9] "Lunar Reconnaissance Orbiter Camera (LROC)," website. http://lroc.sese.asu.edu/.